2.B: 2.G

Nuclear Physics A258 (1976) 317—340; © *North-Holland Publishing Co., Amsterdam*

THE $^{16}O(d, {}^3He)^{15}N$ REACTION AT 29 MeV: Reaction mechanism and nuclear structure †

M. A. FIRESTONE †† and J. JÄNECKE

Department of Physics, The University of Michigan, Ann Arbor, Michigan 48109, USA

A. DUDEK-ELLIS and P. J. ELLIS

Nuclear Physics Laboratory, Keble Road, Oxford, UK
and
School of Physics and Astronomy,
University of Minnesota, Minneapolis, Minnesota 55455, USA

and

T. ENGELAND

Institute of Physics, University of Oslo, Oslo 3, Norway

Received 18 November 1975

Abstract: The reaction $^{16}O(d, {}^3He)^{15}N$ has been investigated using 29 MeV deuterons, and angular distributions were obtained for levels in ^{15}N up to 10 MeV excitation energy. The measured distributions were subjected to distorted-wave (DWBA), compound nucleus (Hauser-Feshbach) and coupled-channel (CCBA) analyses. Only the strong transitions to the $\frac{1}{2}^-$ ground state and the $\frac{3}{2}^-$ state at 6324 keV exhibit distributions which are well described by DWBA. The spectroscopic factors are in agreement with shell-model estimates. The weak transitions generally show little structure and the spectroscopic factors extracted for these transitions tend to be unreasonably large. Contributions from compound nucleus formation were estimated and found to vary between about 10 % and 100 % of the observed cross sections with an average of the order of 30 %. The CCBA analysis for the transitions to the $\frac{5}{2}_1^+$, $\frac{5}{2}_2^+$ and $\frac{7}{2}^+$ states at 5271, 7155 and 7566 keV, respectively, was performed using the spectroscopic amplitudes from weak coupling shell-model wave functions. Inelastic excitations to one-phonon states in the target and residual nuclei were included. The agreement between calculated and experimental distributions is good for both shape and magnitude, a conclusion which is not disturbed by the addition of small compound nucleus contributions. It is evident that spectroscopic factors extracted for the weak transitions on the basis of a direct one-step reaction mechanism alone are unreliable.

E

NUCLEAR REACTIONS $^{16}O(d, {}^3He)$, $E = 29$ MeV; measured $\sigma(E_{^3He}, \theta)$ for $E_x = 0$ to 10 MeV. Statistical compound nucleus analysis, distorted-wave analysis and coupled channels analysis of $\sigma(\theta)$. Discussion of level density parameters, optical model parameters and of multi-step effects.

† Work supported in part by the US Energy Research and Development Administration, contracts nos. E(11-1)-2167 and AT(11-1)-1764.

†† Now at Computer Sciences Corporation, System Sciences Division, Silver Spring, Maryland 20910.

1. Introduction

Theoretical calculations [see for instance refs. [1-5])] for the doubly magic nucleus ^{16}O predict that the ground-state wave function contains about 10–50 % core excitations composed primarily of two-particle two-hole components. Experimental attempts have been made to measure these contributions by means of single-particle pickup reactions on ^{16}O targets [6-11]). A direct one-step reaction mechanism was assumed for the observed weak transitions to positive parity states in the $A = 15$ system with emphasis on the low-lying $\frac{5}{2}^+$, $\frac{1}{2}^+$ doublet, presumably the result of $1d_{\frac{5}{2}}$ and $2s_{\frac{1}{2}}$ pickup from the various particle-hole components in the ^{16}O ground state. However, in only one of the above experiments [9]) has this doublet been resolved, while in all other analyses spectroscopic factors had to be extracted from the superposition of two adjusted DWBA distributions. More disturbing, however, is the fact that many additional transitions of similar strength to positive parity states in ^{15}N and ^{15}O are now known up to about 10 MeV. These could also be the result of pickup from the 2s-1d shell. A further problem is the transition to the $\frac{7}{2}^+$ state at 7566 keV in ^{15}N for which a direct pickup would require $1g_{\frac{7}{2}}$ components in the ground-state wave function of ^{16}O. These are presumably very small because of the large energy difference between the $1g_{\frac{7}{2}}$ and $1p_{\frac{1}{2}}$ orbitals, yet this transition is as strong as most of the other transitions to positive parity states.

It was considered worthwhile in view of the above observations to reinvestigate the ^{16}O(d, ^{3}He)^{15}N reaction with emphasis on the weak transitions and to study the contributions from various reaction mechanisms. First, we estimated the cross sections obtained under the assumption that the reaction proceeds by the formation of a compound nucleus. Although absolute values are difficult to obtain due to uncertainties in level densities, it became apparent that additional processes are necessary to explain the experimental data. Second, we studied the influence of multi-step processes using the coupled-channels Born approximation (CCBA). This is an extension of the traditional distorted-wave Born approximation (DWBA) analysis of stripping or pickup reactions which assumes that the final state in the residual nucleus is reached directly by the transfer of particles to or from the target ground state. In addition to this direct process, the CCBA allows inelastic excitations of the target nucleus before transfer and of the residual nucleus after transfer has taken place. It has generally been found [see for instance refs. [12-17])] that inelastic processes play a particularly important role in those cases where the direct transfer is weak. This is relevant to the present ^{16}O(d, ^{3}He)^{15}N reaction where the approximate shell closure of the ^{16}O target leads to weak cross sections, except for $1p_{\frac{1}{2}}$ and $1p_{\frac{3}{2}}$ pickup populating the ground state and 6324 keV state in ^{15}N. Our CCBA calculations were performed by including the effect of inelastic excitations to one-phonon states in ^{16}O and ^{15}N and by using the spectroscopic amplitudes from weak coupling shell-model wave functions of Ellis, Engeland and coworkers [4, 18]).

In sect. 2 we discuss the experimental procedures and results. The statistical com-

pound nucleus analysis, distorted-wave analysis and coupled-channels analysis are presented in sects. 3, 4 and 5, respectively, followed by a short summary.

2. Experimental procedures and results

Angular distributions for ^{3}He particles from the (d, ^{3}He) reaction on ^{16}O were measured for the range $\theta_{lab} = 12°$ to 45° using a 29.0 MeV deuteron beam from The University of Michigan 83 inch cyclotron. Details of the cyclotron system and beam preparation and analyzing magnets have been previously reported [19]).

Most angular distributions were measured with a gas target and a solid state detector telescope in the scattering chamber. The target was natural oxygen gas (99.7 % ^{16}O) at a pressure of 300 Torr which was contained in a gas cell (radius 30 mm and height 20 mm). A Havar foil of thickness 2.3 μm ($\approx$ 2 mg/cm^2) subtended 270° of the cell and comprised the entrance and exit windows. Two collimating slits are required for the outgoing particles to define the solid angle and to assure that reactions originating from the window are not detected. The front slit was 1.0 mm wide

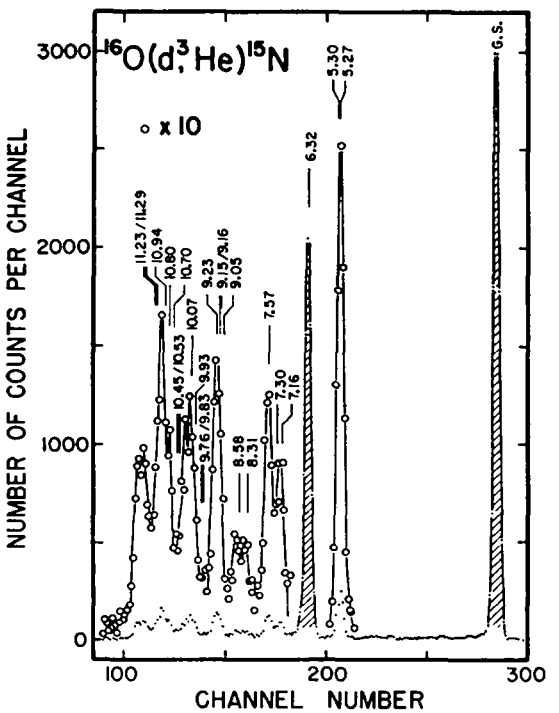

Fig. 1. Energy spectrum for ^{3}He particles from the ^{16}O(d, ^{3}He)^{15}N reaction obtained with a gas target and a solid state detector telescope at $\theta_{lab} = 30°$. Excitation energies in ^{15}N are indicated in units of MeV. All lines except for the two strong lines at 0.0 and 6.32 MeV (shaded) are multiplied by a factor of ten.

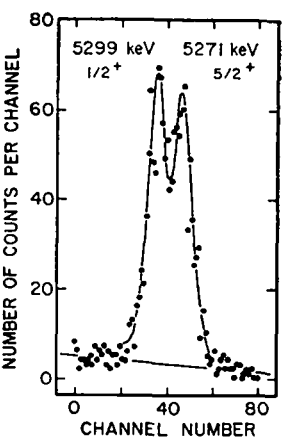

Fig. 2. Energy spectrum for the transition to the 5271 keV $\frac{5}{2}^{+}$ and 5299 keV $\frac{1}{2}^{+}$ doublet obtained with a solid target and magnetic analysis at $\theta_{lab} = 15°$.

and 25.4 mm high, positioned 47.0 mm from the center of the cell. The back slit was approximately 3 mm wide and 5 mm high (total area 14.13 mm^2) located 175.0 mm from the center of the cell in front of the detector telescope. The standard ΔE-E arrangement consisted of Ortec surface barrier silicon detectors of thickness 58 and 410 μm and use was made of the Berkeley Particle Identifier System [20]) for particle identification. The energy resolution was typically about 150 keV. Differential cross sections were obtained from the measured yield by using the geometrical corrections for gas-cell geometry of Silverstein [21]). In addition, the possible effects of slit scattering, beam divergence, and multiple scattering from the Havar window were investigated. It was found that all of these effects contribute at most a few percent to the systematic error in the absolute cross sections. A peak fitting program [22]) was used to extract the intensities of poorly resolved transitions. A more detailed description of resolution and yield corrections and a treatment of errors is given elsewhere [23]). A typical ^{16}O(d, ^{3}He)^{15}N energy spectrum obtained with the gas cell counter telescope system is shown in fig. 1. The lines are labeled by the respective ^{15}N states.

The above system was not adequate to resolve the transitions to the 5271 keV $\frac{5}{2}^+$ and 5299 keV $\frac{1}{2}^+$ states. A solid target and magnetic analysis was therefore used. A self-supporting Al_2O_3 target approximately 80 μg/cm^2 thick was prepared by anodization of aluminum foil [24, 25]). The ^{3}He particles from the reaction were detected by means of a position sensitive solid state detector in the focal plane of the first analyzing magnet. The angular divergence of the incident beam had to be reduced to limit its contribution to kinematic broadening. The energy resolution of about 25 keV was sufficient to resolve the doublet and a spectrum is shown in fig. 2. For additional accuracy the spectra were decomposed by a peak fitting program [26]). Angular distributions were extracted by using only intensity ratios and normalizing them to the unresolved gas cell data. This method removed some of the uncertainties in target thickness, solid angle, and peak fitting.

Angular distributions were obtained for all states in ^{15}N up to 10 MeV excitation with only a few high-lying states unresolved. All distributions are shown in figs. 5 and 6 (see also figs. 3, 7, 10 and 12) together with theoretical curves which are discussed in the following sections.

3. Statistical compound nucleus analysis

Assuming a statistical compound nucleus reaction mechanism, energy averaged angular distributions are evaluated by the Hauser-Feshbach [27]) formula

$$\overline{\frac{\mathrm{d}\sigma_{\alpha\alpha'}(\theta)}{\mathrm{d}\Omega}} = \sum_L \frac{1}{4k_\alpha^2} \sum_{J\pi} \frac{1}{(2I+1)(2i+1)} \Bigg\{ \sum_{ls} \sum_{l's'} \frac{T_l(\alpha) T_{l'}(\alpha')}{\sum_{\alpha''l''s''} T_{l''}(\alpha'')} \times (2l+1)(2l'+1)(2J+1)^2 W(llJJ; Ls) W(l'l'JJ; Ls') \times \langle l0l0|llL\rangle \langle l'0l'0|l'l'L\rangle (-1)^{s-s'} P_L(\cos\theta) \Bigg\}, \quad (1)$$

with $0 \leqq L \leqq \min(2l, 2l', 2J)$. Here, unprimed and primed quantities refer to the incoming and outgoing channels, respectively. The W and $\langle\ |\ \rangle$ are Racah and Clebsch-Gordan coefficients, respectively, and the T_l are transmission coefficients. For the entrance channel α, the target spin $\boldsymbol{I}$ and projectile spin $\boldsymbol{i}$ are coupled to the channel spin s which in turn is coupled with the orbital angular momentum $\boldsymbol{l}$ to give a total angular momentum of $\boldsymbol{J}$. Clearly this must be the spin of the compound nucleus. The angular distributions are symmetric about 90° since the expression vanishes for odd L.

In order to evaluate the denominator $\sum_{\alpha''l''s''} T_{l''}(\alpha'')$ of eq. (1), a knowledge of the transmission coefficients for all possible decay channels α'' is in principle required. However, to a good approximation only the most important channels such as nucleon and α-particle emission need to be considered. Furthermore, at higher bombarding energies the major contributions to the sum come from highly excited states and it is sufficient to replace the sum over individual levels by an integral involving level densities. In the present work the analytic expression for $\sum_{\alpha''l''s''} T_{l''}(\alpha'')$ of Eberhard *et al.* [28]) was employed. Since an accurate knowledge of the level densities of the residual nuclei is required to make reasonable cross-section predictions, the characteristics of these level densities will be discussed below.

At excitation energies below about 10 MeV, level densities are usually well described [29]) by an expression where a constant nuclear temperature T is assumed, namely

$$\rho(E_x) = \frac{N(E_x)}{T} = \frac{1}{T} \exp\left[\frac{E_x - E_0}{T}\right]. \tag{2}$$

Here, $N(E_x)$ is the total number of levels up to the excitation energy E_x, and E_0 is a constant (related to the pairing energy). Level densities at higher excitation energies are generally assumed to be described by the Fermi-gas model. One commonly used formula is that of Gilbert and Cameron [30])

$$\rho(E_x) = \tfrac{1}{12}\sqrt{\pi}\, \frac{\exp[2\sqrt{aU}]}{a^{\frac{1}{4}} U^{5/4}} \frac{1}{\sqrt{2\pi}\,\sigma}. \tag{3}$$

Here, $U = E_x - \Delta$ is an effective excitation energy with pairing corrections [30]) subtracted, a is a level density parameter, and σ a spin distribution parameter which is related to the nuclear moment of inertia and the nuclear temperature. Gilbert and Cameron [30]) have also given an expression for the spin dependence of the level densities which is used in the present work. The relative distribution of states with different spins and parities J^π depends strongly on the spin distribution parameter σ while the observable level densities for states with all values of J^π [eqs. (2) or (3); note that the level degeneracy of $2J+1$ for every value of J due to the magnetic quantum number is still included] are independent or only weakly dependent on σ.

Some uncertainty exists about nuclear level densities and their parameterization. The transition to the $\frac{7}{2}^+$ state at 7566 keV was therefore chosen to evaluate differential

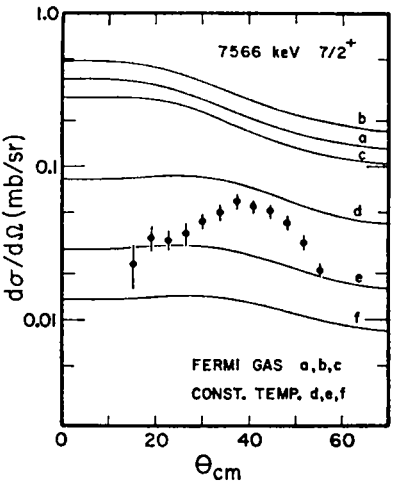

Fig. 3. Experimental and calculated compound nucleus angular distributions for the transitions to the 7566 keV $\frac{7}{2}^+$ state. Curves (a), (b) and (c) are based on Fermi-gas model level densities (using parameter sets A, B and C of table 1, respectively). Curves (d), (e) and (f) are based on constant-temperature level densities (parameter set D of table 1). Curves (e) and (f) were obtained with increased spin distribution parameters σ (see text).

TABLE 1

Parameters [a]) for the Fermi-gas model and constant-temperature model level density formulae

	^{17}F	^{17}O	^{14}N	^{18}F			Parameter set	Ref.
Fermi-gas model								
a/A (MeV^{-1})	0.151	0.151	0.152	0.152			A	[32])
Δ (MeV)	2.67	2.46	0.0	0.0				
σ	2.209	2.261	2.071	2.544	$J_{max} = 10$	$\Gamma =$ 583 keV		
a/A (MeV^{-1})	0.156	0.150	0.134	0.166			B	[30,31])
Δ (MeV)	2.5	2.4	0.0	0.0				
σ	2.195	2.267	2.138	2.488	$J_{max} = 10$	$\Gamma =$ 208 keV		
a/A (MeV^{-1})	0.185	0.185	0.127	0.155			C	this work
Δ (MeV)	3.15	3.20	0.0	0.0				
σ	2.088	2.133	2.168	2.532	$J_{max} = 9$	$\Gamma =$ 1015 keV		
Constant-temperature model								
T (MeV)	2.170	2.170	3.194	2.636			D	this work
E_0 (MeV)	1.038	1.038	0.124	−3.024				
σ	1.913	1.913	1.975	2.211	$J_{max} = 7$	$\Gamma =$ 294 keV		
σ [b])	2.209	2.261	2.071	2.544	$J_{max} = 7$	$\Gamma =$ 294 keV		
σ [c])	2.706	2.706	2.793	3.127	$J_{max} = 7$	$\Gamma =$ 294 keV		

[a]) a/A, Δ, T and E_0 are independent parameters; σ, J_{max} and Γ are calculated [28]).
[b]) $\sigma^2 = \sigma^2$ (set A) used for curve (e).
[c]) $\sigma^2 = 2\sigma^2$ (set D) used for curve (f).

cross sections using different assumptions. The results are shown in fig. 3. Curves (a), (b) and (c) are based on the Fermi gas model and curves (d), (e) and (f) on the constant temperature model. The parameters a/A and Δ used with eq. (3) and T and E_0 used with eq. (2) are listed in table 1. Also listed in the table are, for each parameter set, several derived quantities [28, 33]) namely the various spin distribution parameters σ, the yrast-level spin cutoff value J_{max} and the calculated compound nucleus level width Γ (see below). Curves (a), (b) and (c) of fig. 3 show the results using parameter sets A, B and C of table 1. Sets A and B are from the literature [30-32]) while set C was obtained by matching at $E_{exc} \approx 10$ MeV the Fermi-gas and constant temperature expressions, the latter being determined from the known low-energy level densities. Curves (d), (e) and (f) of fig. 3 show the results based on parameter set D. Only curve (d), however, was obtained by using the required values [28]) for the spin distribution parameter σ ($\sigma^2 = \mathscr{I}_{rigid} T/\hbar^2$; $\mathscr{I}_{rigid}$ is the rigid body moment of inertia and T the thermodynamic temperature) whereas increased values were used for curves (e) and (f) as discussed below. Fig. 3 shows that curves (a)–(c) over-estimate the observed forward angle cross sections by more than an order of magnitude and even curve (d) which is based on the assumption of much higher level densities is too high by a factor of four or more. The shape of the observed distribution is also not reproduced.

Additional information about proper level densities can be obtained from a comparison between calculated and experimental compound nucleus level widths. Widths were calculated from [33])

$$\Gamma_J = (2\pi\rho_J)^{-1} \sum_{\alpha'' l'' s''} T_{l''}(\alpha''), \tag{4}$$

where ρ_J is the level density of the compound nucleus, and the sum over the transmission coefficients is again obtained from the expressions of Eberhard *et al.* [28]). For $E_{exc} \approx 33$ MeV in the compound nucleus ^{18}F the J-averaged calculated widths are 580, 210, 1010 and 290 keV for the level densities based on parameter sets A–D of table 1, respectively. The dependence on J is only weak. An extrapolated experimental value was obtained from the results of level density fluctuation analyses [34]) in conjunction with the approximate relationship [35])

$$\Gamma \approx \Gamma_0 \exp(-\alpha\sqrt{A/E_x}). \tag{5}$$

The result of $\Gamma \approx 440$ keV is best compatible with the predictions from the Fermi-gas model using set A and with the constant temperature model using set D. However, since the experimental forward-angle cross sections of $\lesssim 20$ μb/sr are strongly over-estimated, it was decided to further investigate the dependence of the calculated cross sections on the yrast-level cutoff value J_{max} and on the spin distribution parameter σ by treating them as adjustable parameters.

Fig. 4a shows the calculated 0° cross sections as a function of J_{max} for constant σ^2. Fig. 4b shows the dependence on σ^2 for constant J_{max}. The filled circles represent the 0° cross sections of curves (a) and (d) of fig. 3. No reasonable modification of the

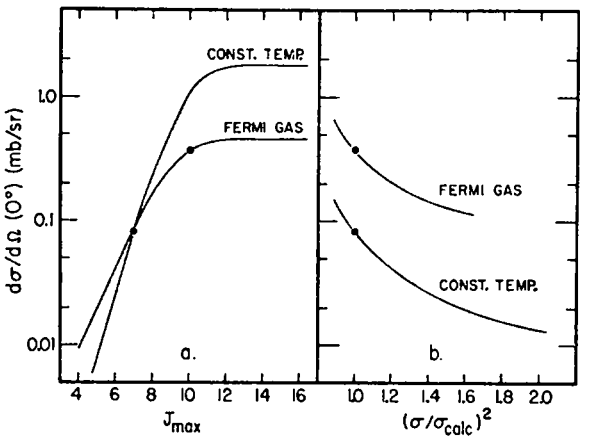

Fig. 4. Calculated 0° compound nucleus cross sections for the transition to the 7566 keV $\frac{7}{2}^+$ state as a function of J_{max} and σ^2, respectively. The curves are obtained for assumed level densities from the Fermi-gas model and from the constant-temperature model (parameter sets A and D of table 1 with variations in J_{max} and σ^2). The filled circles are the cross sections from curves (a) and (d) of fig. 3, respectively.

values for σ and J_{max} from set A in table 1 leads to sufficiently reduced Fermi-gas model cross-section estimates. The constant temperature model cross-section estimates, however, are much more sensitive to changes in σ or J_{max} from set D in table 1. Decreasing J_{max} by one or two units or increasing the spin distribution parameter σ by a factor of about $\sqrt{2}$ leads to forward-angle cross sections compatible with the experimental data. Curve (f) in fig. 3 (see also fig. 5) was obtained with the assumption $\sigma^2 = 2\sigma^2$(set D). Increasing σ only according to $\sigma^2 = \sigma^2$ (set A) (curve (e)) was not sufficient.

It was concluded that the use of constant temperature level densities with spin distributions parameters σ^2 increased by a factor of two over the values calculated from $\sigma^2 = \mathscr{I}_{rigid}T/\hbar^2$ (more high-spin states at the expense of low-spin states) results in realistic compound nucleus cross-section estimates. While this procedure is essentially equivalent to an arbitrary renormalization, it is reassuring to find that our conclusions are supported by other work [36-38]). Maruyama [36]) and Grimes *et al.* [37]) found that near closed shells the constant temperature model yields better results than the Fermi-gas model. Ayik and Ginocchio [38]) concluded recently that the Fermi-gas model underestimates the density of states with higher angular momentum in the 2s-1d shell.

The Fermi-gas model level densities with parameter set A, the constant-temperature model level densities with parameter set D and with $(\sigma/\sigma_{calc})^2$ equal to one and to two (corresponding to curves (a), (d) and (f) of fig. 3) were used to calculate angular distributions from eq. (1) for essentially all experimentally observed weak transitions. Optical model transmission coefficients derived from parameter sets A and B of table 2 were used for incoming and outgoing channels. The results are shown

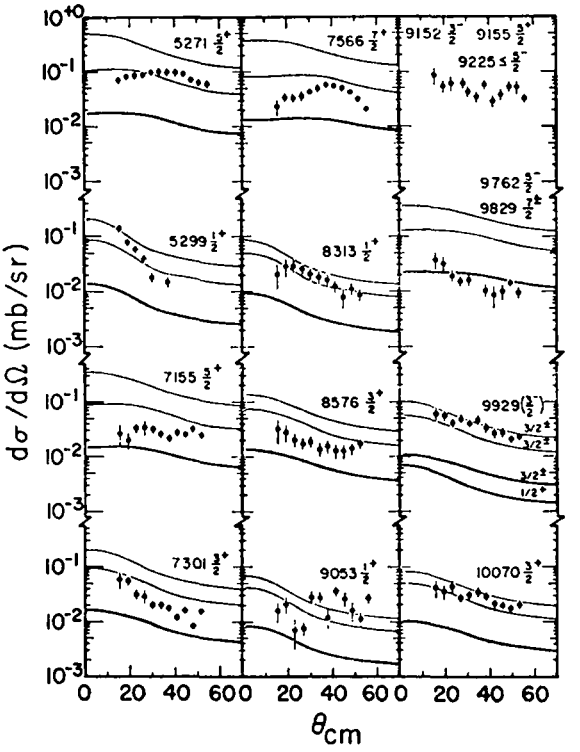

Fig. 5. Experimental angular distributions for the "weak" transitions and calculated compound nucleus angular distributions based on Fermi-gas model level densities (upper thin lines), on constant-temperature model level densities (lower thin lines) and on constant-temperature model level densities with $(\sigma/\sigma_{calc})^2 = 2$ (thick lines). Excitation energies are in units of keV. The error bars reflect statistical uncertainties and uncertainties in background subtraction and peak fitting.

in fig. 5. No distributions were calculated for the unresolved triplet of states near 9200 keV. The parity of the state at 9829 keV is uncertain but does not significantly affect the predicted angular distributions for the unresolved doublet near 9800 keV. Spin and parity of the state at 9929 keV are uncertain and the curves are labeled by the assumed values.

The curves based on constant-temperature level densities with $(\sigma/\sigma_{calc})^2 = 2$ (heavy lines) do not exceed the data for any of the transitions and are therefore believed to constitute reliable estimates of the contributions from compound nucleus formation. Only the transitions to the unresolved doublet near 9800 keV appears to be populated primarily by a compound nucleus mechanism. The contributions for the other transitions vary, and the average is of the order of about 30 % of the observed cross sections. The shapes of some observed transitions (particularly for the states at 5271, 5299 and 7566 keV) are not compatible with the calculated shapes. Thus, it appears that direct processes are required to explain most of the experimentally observed cross sections.

4. Distorted-wave analysis

Figs. 6 and 7 show the experimental angular distributions for transitions to states in ^{15}N up to an excitation energy of 10 MeV and the respective DWBA curves calculated with the computer code DWUCK [39]). Three distributions to highly excited

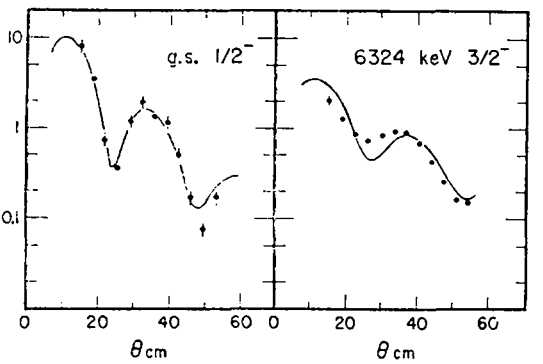

Fig. 6. Experimental angular distributions for the transitions to the $\frac{1}{2}^-$ ground state and $\frac{3}{2}^-$ state at 6324 keV. The curves are DWBA predictions.

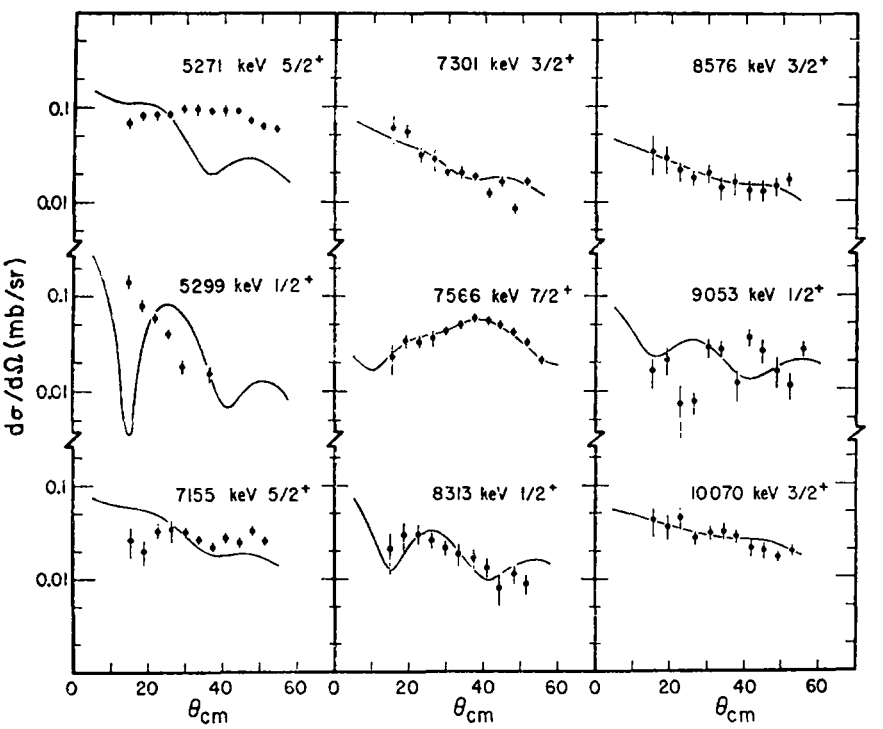

Fig. 7. Experimental angular distributions for the "weak" transitions to resolved states with unique spin-parity assignments. The curves are DWBA predictions.

unresolved states or states with uncertain spin-parity assignments are not included. The optical parameters for the deuterons and ^{3}He particles as well as the parameters used to calculate the bound state wave functions are listed in table 2. The imaginary strengths taken for the DWBA analysis are given in parenthesis and the parameter β_3 was not used. Further discussion of the parameter sets are given in sect. 5. The DWBA curves shown in figs. 6 and 7 are based on parameter sets A, B and D of table 2. The distributions (not shown) and spectroscopic factors based on sets A, C and D are quite similar.

The angular distributions for the two strong transitions to the $\frac{1}{2}^-$ ground state and the $\frac{3}{2}^-$ state at 6324 keV are shown in fig. 6. They are reproduced quite well by the respective DWBA curves. The angular distributions for the "weak" transitions are shown in fig. 7. The shapes of almost half of the distributions are not compatible with DWBA predictions. Spectroscopic factors were deduced from the comparison between experimental and calculated distributions disregarding the quality of the fits and are included in table 3, col. 11 despite obvious uncertainties. This table lists all spectroscopic factors obtained for single-particle pickup reactions on ^{16}O, both from experimental investigations (cols. 4–11) and from theoretical investigations (cols. 12–15).

The spectroscopic factors (col. 11) for the two strong transitions are 30–40% larger than the closed shell estimates of $2j+1 = 2$ and 4, respectively. They are also larger than the values obtained in the other experimental and theoretical investigations. The extracted spectroscopic factors appear insensitive to the optical model parameters chosen. A possible source of the discrepancy lies in the neglect of multi-step processes. The coupled-channels analysis of sect. 5 shows (see fig. 10) that the inclusion of such processes enhances the calculated peak at 35° for the $\frac{1}{2}^-$ ground state significantly while the overall fit to the data, however, is somewhat poorer.

Table 3 shows a fairly wide scatter in the various results for the 5271 keV $\frac{5}{2}^+$ and 5299 keV $\frac{1}{2}^+$ doublet. The experimental and theoretical spectroscopic factors for the $\frac{5}{2}^+$ level seem to cluster around a value of about 0.2. A more detailed comparison is not useful since multi-step processes are found to be important (see sect. 5). The spectroscopic factors for the $\frac{1}{2}^+$ level are smaller. A value of about 0.05 seems to be preferred by experiment and an even smaller value by theory. It may be noted that the measured angular distribution for the $\frac{1}{2}^+$ state, though strongly forward peaked, does not resemble the predicted DWBA curve for $l = 0$. Thus, this transition also suggests interference from multi-step processes. The only previous experiment to resolve the $\frac{5}{2}^+$ and $\frac{1}{2}^+$ doublet was that of Purser *et al.* [9]) in which the (d, ^{3}He) and (d, t) reactions were studied at $E_d = 20$ MeV. Their extracted spectroscopic factor for the $\frac{1}{2}^+$ level is close to our value but that for the $\frac{5}{2}^+$ level is much smaller.

The angular distributions for the levels at higher excitation energy tend to be rather structureless since Coulomb effects dampen the oscillations at these energies. The extracted spectroscopic factors are larger than those predicted by theory, although

TABLE
Parameters of the

	V (MeV)	r_V (fm)	a_V (fm)	W [b]) (MeV)	W' [b]) (MeV)	r_W (fm)
d+^{16}O	73.6	1.25	0.75		7.80 (13.00)	1.3
^{3}He+^{15}N	162.8	1.23	0.60	9.33 (12.44)		1.8
^{3}He+^{15}N	122.9	1.21	0.65	11.25 (15.00)		1.7
bound state	[a])	1.25	0.65			

[a]) Adjusted to reproduce measured separation energy.

TABLE
Experimental and theoretical spectroscopic

E_x(^{15}O) (keV)	E_x(^{15}N) (keV)	J^π	(d, ^{3}He) 20 MeV [c])	34.4 MeV [f])	82 MeV [g])	52 MeV [a, h])	(p, d) 45.3 MeV [a, i])
0	0	$\frac{1}{2}^-$	2.10	2.30	2.50	2.18	1.8 ±0.1
5242	5271	$\frac{5}{2}^+$	0.036	0.31	0.05–0.10	0.16±0.04	0.11±0.01
5181	5299	$\frac{1}{2}^+$		0.038	0.007–0.02	0.10±0.07	0.02±0.01
6177	6324	$\frac{3}{2}^-$		3.64	3.60	3.32	2.6 ±0.2
6859	7155	$\frac{5}{2}^+$					0.02±0.01
6788	7301	$\frac{3}{2}^+$					0.02±0.01
7276	7566	$\frac{7}{2}^+$					≲ 0.03±0.01
7552	8313	$\frac{1}{2}^+$					
8283	8579	$\frac{3}{2}^+$					0.01±0.005
8739	9053	$\frac{1}{2}^+$					
8978	9152	$\frac{3}{2}^-$					0.04±0.02
8920	9155	$\frac{5}{2}^+$					
8920	9225	$\frac{1}{2}^-$					
9483	9762	$\frac{5}{2}^-$					
9660	9829	$(\frac{7}{2}^-)$					
9606	9929	$\frac{3}{2}^-, (\frac{1}{2}, \frac{3}{2})^+$				0.26($\frac{3}{2}^-$), 0.59$(\frac{3}{2})^+$	0.18±0.03
≈9500	10070	$\frac{3}{2}^+$					

[a]) Additional spectroscopic strength observed for transitions to states between 10 and 11 MeV.
[b]) Relative spectroscopic factors.
[c]) Private communication; reported in ref. [11]).

both are generally small. The weak coupling model predicts significant amounts of 1p strength at about 9 MeV. This excitation energy appears to be too low and possible candidates for such strength are the 9929 keV state seen in the present and other experiments [10, 11]) and states at higher excitation energy [10, 11]). It is noteworthy that if the 7566 keV $\frac{7}{2}^+$ state is assumed to be populated by $1g_{\frac{7}{2}}$ transfer, a spectroscopic

2
optical model potentials

a_W (fm)	$V_{s.o.}$ (MeV)	$r_{s.o.}$ (fm)	$a_{s.o.}$ (fm)	β_3	r_c (fm)	Parameter set
0.75	6.0	1.13	0.75	0.6	1.3	A
0.86				0.25	1.3	B
0.90	5.5	1.11	0.60	0.25	1.4	C
	7.5	1.25	0.65		1.2	D

[b]) The larger values in parentheses were used in the DWBA analysis.

3
factors C^2S for pickup reactions on ^{16}O

(d, t) at 20 MeV [e])	(^{3}He, α) at 11 MeV [j])	(d, ^{3}He) at 29 MeV [k])	ZBM model [l])	Wong model [d]) central force [m])	Wong model [d]) realistic force [m])	Ellis and Engeland weak coupling model [n])
1.5	1.00 [b])	2.60	1.45, 1.60 [c])	1.85	1.85	1.51
0.043	0.58	0.26	0.18, 0.35 [c])	0.20	0.10	0.17
0.027	0.22	0.06	0.04 [c])	0.0	0.0	0.004
3.1	2.11	5.60		2.95	2.85	2.90
	1.03	0.12				0.014
	0.60	0.21		0.07	0.10	0.007
		0.45				
		0.08				0.010
		0.18				0.013
		0.10				negligible
						0.57
						0.011
						0.21
	0.71($\frac{3}{2}^-$), 0.10($\frac{1}{2}^+$), 0.34($\frac{3}{2}^+$)					0.007
	0.34					0.001

[d]) All values are summed spectroscopic strengths.
[e]) Ref. [9]). [f]) Ref. [6]). [g]) Ref. [8]). [h]) Ref. [11]). [l]) Ref. [10]). [j]) Ref. [7]).
[k]) This work. [l]) Ref. [2]). [m]) Ref. [3]). [n]) Refs. [4, 18]) and this work.

factor of 0.45 is required, which is clearly unreasonable. The conclusions from the present DWBA analysis, in conjuction with the results from the earlier analysis (sect. 3) based on a statistical compound nucleus reaction mechanism, clearly demonstrate the importance of multi-step processes for those transitions which have relatively small cross sections.

5. Coupled-channels analysis

5.1. DESCRIPTION OF THE CALCULATIONS

In this section we study the effect of multi-step processes on the predicted cross section using the coupled-channels Born approximation (CCBA) which allows inelastic excitations before and after the transfer of a particle. In our model we take into account the inelastic excitation of the one phonon 3^- state at 6131 keV in ^{16}O and of the 5271 keV $\frac{5}{2}^+_1$ and 7566 keV $\frac{7}{2}^+$ states in ^{15}N which we view as a $1p_{\frac{1}{2}}$ hole coupled to a 3^- phonon. While this model probably represents inelastic scattering reasonably well when fitted to the data, the assumption that only a $1p_{\frac{1}{2}}$ nucleon is transferred is not in accord with microscopic calculations. We therefore felt it more reasonable to allow all possible 1p and 2s-1d transfers using spectroscopic amplitudes generated from microscopic shell-model calculations [4, 18]).

The processes considered are illustrated in fig. 8a. Note that the direct population of the $\frac{7}{2}^+$ level demands $1g_{\frac{7}{2}}$ transfer whereas the structure of nuclei in this region has been quite satisfactorily described [see for instance refs. [2-5, 18, 40])] by using only the single-particle states of the 1p and 2s-1d shells. We therefore take this spectroscopic amplitude to be zero. For the $\frac{5}{2}^+$ levels in ^{15}N the octupole strength appears to be fragmented. We have therefore carried out the separate calculation indicated in fig. 8b to obtain the cross section of the 7155 keV $\frac{5}{2}^+_2$ level. Inelastic excitations may well be important in other cases too, but since no natural macroscopic model presents itself we have not initiated calculations beyond the ones outlined above.

The formalism used to take into account the effect of the inelastic scattering processes is the source-term method which has been extensively discussed by Ascuitto and Glendenning [41]) and by Edens [42]). This method involves solving first the coupled equations for ^{16}O(d, d′) inelastic scattering subject to the boundary condition that

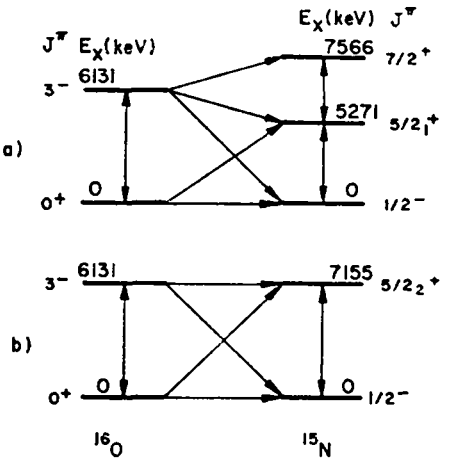

Fig. 8. Direct and indirect processes considered in the coupled-channels analysis for populating states in ^{15}N via the ^{16}O(d, ^{3}He)^{15}N reaction.

there are incoming waves only in the channels with ^{16}O in its ground state. The resulting wave functions are then used to construct the source term which gives the feeding of the various levels in ^{15}N due to the pickup process. A zero-range stripping interaction is assumed, with the strength taken from ref. [43]). Finally, the source term is inserted in the coupled equations representing inelastic scattering of ^{3}He particles on ^{15}N in its ground state, and the set of inhomogeneous coupled equations is solved subject to the boundary condition that there are only outgoing waves. The matching of the wave functions onto the asymptotic forms yields the scattering matrix elements in the usual way. This CCBA calculation takes into account inelastic scattering to all orders, but the transfer process is assumed to be sufficiently weak that it can be treated in first order only. If a single level is selected in the entrance and exit channels, the DWBA cross section is obtained. The code DWUCK [39]) was again used to generate the DWBA results.

A number of parameters need to be specified in order to carry out the calculations. First we consider briefly those parameters which describe the inelastic scattering in the entrance and exit channels. Since the nuclei we discuss are thought to be spherical, we assume that the coupling between the states considered is due to vibrational deformations of the nuclear shape. The formalism is well known [see for instance ref. [44])].

The optical model potential was used in the form

$$U_{\mathrm{opt}}(r, \theta, \varphi) = Vf(r, R_V, a_V) + i[Wf(r, R_W, a_W) + W' g(r, R_W, a_W)] + V_{\mathrm{s.o.}} h(r, R_{\mathrm{s.o.}}, a_{\mathrm{s.o.}}) \boldsymbol{l} \cdot \boldsymbol{s} + V_{\mathrm{C}}(r, R_{\mathrm{c}}), \qquad (6)$$

where

$$f(r, R_x, a_x) = -(1+E_x)^{-1}, \quad g(r, R_x, a_x) = -4E_x(1+E_x)^{-2},$$

$$h(r, R_x, a_x) = -bE_x(a_x r)^{-1}(1+E_x)^{-2}, \quad E_x = \exp[(r-R_x)/a_x],$$

with $b = 4.0$ fm^2. The nuclear surface was allowed to vibrate about a spherical shape according to

$$R_x = R_{0x}\left\{1 + \sum_{\lambda\mu} \frac{\beta_\lambda}{(2\lambda+1)^{\frac{1}{2}}} ((-1)^\mu b^+_{\lambda-\mu} + b_{\lambda\mu}) Y_{\lambda\mu}(\theta, \varphi)\right\}, \qquad (7)$$

with $R_{0x} = r_x A^{\frac{1}{3}}$. Here b^+ and b are phonon creation and destruction operators. In the present work we restrict our attention to the octupole phonon excitation, i.e. $\lambda = 3$. Eq. (7) for R_x was inserted in the real and imaginary parts of the optical potential of eq. (6) and the resulting expression was expanded in powers of the parameter β_λ. Terms through second order were retained. A spherical spin-orbit potential was used. A negligible effect was found when the Coulomb potential was allowed to vibrate so that a uniform spherical charge distribution was used with $R_{\mathrm{c}} = r_{\mathrm{c}} A^{\frac{1}{3}}$.

Two levels in ^{16}O were considered for the ^{16}O(d, d') reaction, the zero-phonon ground state $|0\rangle$ and the one-phonon 3^- state, $b^+_{3\mu}|0\rangle$ at 6131 keV. It is then straightforward to obtain the coupling matrix elements. In order to ensure that our

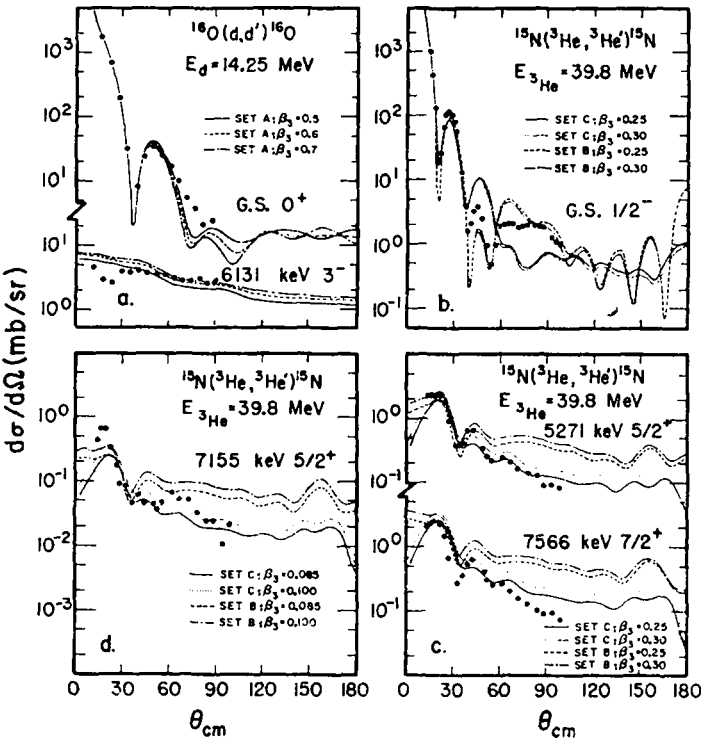

Fig. 9. Experimental angular distributions for elastic and inelastic deuteron scattering on ^{16}O [(a): data from ref. [45])] and for elastic and inelastic ^3He scattering on ^{15}N [(b)–(d): data from ref. [50])]. The optical parameter sets and vibrational parameters β_3 used in the coupled-channel calculations are indicated.

choice of parameters was reasonable, we carried out coupled-channel calculations and compared the results with the inelastic scattering data of Nguyen [45]) taken at a bombarding energy of E_d = 14.25 MeV. The average optical model parameters of Hinterberger *et al.* [46]) were used adopting the energy dependence cited there. After adjustment of the imaginary and spin-orbit parameters, the results of fig. 9a were obtained for β_3 values of 0.5, 0.6 and 0.7. The value β_3 = 0.5 appears to be somewhat favored, although the shape of the 3^- cross section is not well given. A recent DWBA analysis [47]) of other (d, d') data gave a value of 0.33, whereas the (α, α') work of Harvey *et al.* [48]) yielded a larger value of about 0.67, and the γ-decay width of the 6131 keV level results in a still larger value [49]). We adopted a value of β_3 = 0.6. Since a higher bombarding energy of E_d = 29 MeV was used in the present experiment we applied a small correction to the real well depth following ref. [46]). Thus, parameter set A of table 2 was obtained for use in the reaction calculations. In the DWBA calculations with pure elastic scattering in the entrance channel, the increased values for W' given in parenthesis were used as remarked previously.

The coupling of three levels in ^{15}N was considered for the ^{15}N(^{3}He, ^{3}He′) reaction. These states were the $\frac{1}{2}^-$ ground state regarded as a $1p_{\frac{1}{2}}$ hole in the ^{16}O core, and the 5271 keV $\frac{5}{2}^+_1$ and 7566 keV $\frac{7}{2}^+$ states regarded as $1p_{\frac{1}{2}}$ holes coupled to a 3^- vibration. It should be noted that microscopic shell-model calculations [4, 18]) suggest that this description is quite reasonable for the $\frac{5}{2}^+$ level, but less so for the $\frac{7}{2}^+$ level. On the other hand, the similarity of the measured (^{3}He, ^{3}He′) angular distributions [50]) as well as the (α, α') angular distributions [51]) suggests some common inelastic excitation mechanism for which the phonon picture may be a reasonable parameterization.

Figs. 9b and 9c show the comparison between the experimental data of Ball and Cerny [50]) taken at $E_{^3\mathrm{He}} = 39.8$ MeV and the coupled-channel calculations using two sets of optical parameters and two values for the vibrational parameter, $\beta_3 = 0.25$ and 0.30. The first set labeled B utilizes the elastic optical model parameters of ref. [50]). The strength W was reduced by 25 % in order to obtain roughly the same elastic cross section when the inelastic channels were explicitly included. The second set labeled C was chosen so that unlike set B the volume integral J_R of the real part of the potential was similar to that for the deuteron parameters ($J_R \approx 450$ MeV · fm^3). Set B gives better results with little sensitivity to β_3 for the elastic scattering data of fig. 9b. Set C gives somewhat better agreement for the inelastic data of fig. 9c. The forward peak in the cross section for the 7566 keV $\frac{7}{2}^+$ level indicates $\beta_3 = 0.25$ while that for the 5271 keV $\frac{5}{2}^+$ level shows a preference for a slightly larger value. The latter conclusion should be treated with caution though, since a contribution may be present from the nearby unresolved 5299 keV $\frac{1}{2}^+$ level. We adopted the value $\beta_3 = 0.25$, which is much smaller than that obtained in ^{16}O(d, d′). Although this suggests fragmentation of the octupole strength, it may also reflect the projectile dependence of β_3 since the (α, α') data [48]) yielded rather similar values for ^{15}N and ^{16}O. Parameter sets B and C are listed in table 2. A small correction has been applied following ref. [52]) to account for the different ^{3}He energy.

One further fragment of octupole strength appears to be residing in the 7155 keV $\frac{5}{2}^+_2$ state. For this second $\frac{5}{2}^+$ level we used a two-level model by coupling it with the $\frac{1}{2}^-$ ground state as indicated in fig. 8b. The cross sections obtained using parameter sets B and C with values of $\beta_3 = 0.085$ and 0.100 are shown in fig. 9d. It was not possible to fit the magnitude of both the forward peak and the data at larger angles. By focussing on the latter, a value of $\beta_3 = 0.085$ and parameter set C appear to be slightly preferred.

For the reaction calculations we need the form factors of the transferred protons for all the possible transitions indicated in fig. 8. These form factors were taken to be the product of a spectroscopic amplitude and a normalized single-particle wave function calculated in a Woods-Saxon well (set D of table 2) with the depth adjusted to reproduce the observed energy difference between each pair of states considered. Rather than adopt the spectroscopic amplitudes of the phonon model, we have, as remarked, felt it to be more reasonable to use those generated by microscopic shell-model calculations which have yielded a reasonable account of the nuclei in this region. These

TABLE 4
Spectroscopic amplitudes $(C^2S)^{\frac{1}{2}}$ used in the CCBA calculations

^{15}N-^{16}O	$1p_{\frac{1}{2}}$	$1p_{\frac{3}{2}}$	$1d_{\frac{5}{2}}$
$\frac{1}{2}^-$ -0^+	1.228		
$\frac{1}{2}^-$ -3^-			−0.572
$\frac{5}{2}_1^+$-0^+			0.408
$\frac{5}{2}_1^+$-3^-	0.530	−0.033	
$\frac{7}{2}^+$ -0^+			
$\frac{7}{2}^+$ -3^-	0.410	−0.294	
$\frac{5}{2}_2^+$-0^+			0.117
$\frac{5}{2}_2^+$-3^-	0.156	−0.240	

spectroscopic amplitudes based on the weak coupling work of ref.s [4, 18]) are listed in table 4. Care was taken to ensure that the phases were consistent with those chosen for inelastic scattering. An ambiguity arose for the $\frac{5}{2}_2^+$ level since the calculated transition $(B[E3])^{\frac{1}{2}}$ to the ground state was very small. The predicted sign was therefore unlikely to be reliable. We examined both signs and found that only one sign gave a peak in the $\frac{5}{2}_2^+$ reaction cross section at about 25° as observed. This phase was then adopted.

5.2. RESULTS FOR THE $^{16}O(d, ^3He)^{15}N$ REACTION

Using the parameters described above, we have carried out CCBA calculations for the $^{16}O(d, ^3He)^{15}N$ reaction. We first consider the coupling of three levels ($\frac{1}{2}^-$, $\frac{5}{2}_1^+$ and $\frac{7}{2}^+$) in ^{15}N as illustrated in fig. 8a. The results are given in fig. 10. For the $\frac{1}{2}^-$ ground state of ^{15}N we have used parameter set B in the exit channel but very similar results are obtained with set C. The results are also insensitive to small variations of β_3. It is seen from fig. 10 that the inelastic processes included in CCBA change the magnitude of the DWBA cross section significantly. This is mainly due to contributions from the 3^- to $\frac{1}{2}^-$ route transferring a $1d_{\frac{5}{2}}$ particle. As previously remarked this may be the reason for the large spectroscopic factor predicted by DWBA, but still the DWBA gives somewhat better agreement with the shape of the experimental angular distribution.

The data for the 5271 keV $\frac{5}{2}_1^+$ level are in clear disagreement with the DWBA predictions given by the dashed curve in fig. 10, but lie essentially between the CCBA angular distributions obtained with parameter sets B and C. The shape of the angular distribution favors set B, although the predicted peak occurs at too small an angle. The magnitude of the data is better accounted for by set C rather than set B, but we note that the cross section of the 5271 keV $\frac{5}{2}_1^+$ level, unlike that of the $\frac{1}{2}^-$ and of the $\frac{7}{2}^+$ level, is fairly sensitive to the optical model parameters. This is already suggested in fig. 10 and becomes quite apparent when the real well depths are varied. A reduction by 10% of the deuteron potential V reduces the magnitude of the cross

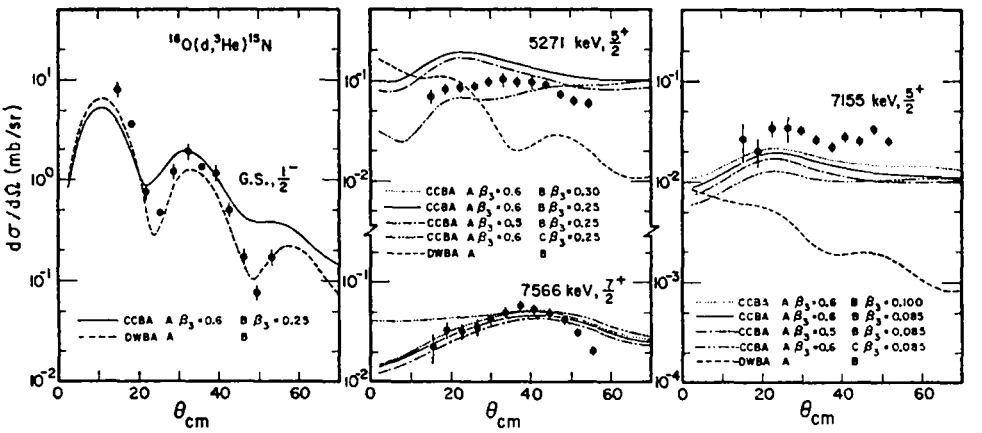

Fig. 10. Experimental and theoretical angular distributions for the transitions to the states at 0 keV $\frac{1}{2}^-$, 5271 keV $\frac{5}{2}_1^+$, 7566 keV $\frac{7}{2}^+$ and 7155 keV $\frac{5}{2}_2^+$. The curves are the result of DWBA and CCBA calculations with the different optical and vibrational parameters indicated.

section obtained with set B by about 30 % and also flattens the shape, thus yielding improved agreement with experiment. In view of this, we regard the CCBA prediction of set B as acceptable while that of set C is not unreasonable. Fig. 10 also indicates the sensitivity to variations of β_3 in the entrance channel. The sensitivity is considerably weaker in the exit channel.

All CCBA results obtained for the 7566 keV $\frac{7}{2}^+$ level, also displayed in fig. 10, show reasonable agreement with the data. A modest sensitivity to β_3 is noted, together with some preference for parameter set B rather than C. We have not allowed a direct $1g_{\frac{7}{2}}$ transfer in obtaining these results, but it is perhaps worth recalling that while the DWBA prediction assuming $1g_{\frac{7}{2}}$ transfer is quite reasonable in shape, the extracted spectroscopic factor is clearly unreasonable.

Since inelastic scattering to the 7155 keV $\frac{5}{2}_2^+$ level of ^{15}N is weak, we have, as discussed previously, adopted a two level model consisting of this second $\frac{5}{2}_2^+$ state together with the ground state of ^{15}N. The processes considered in the reaction are indicated in fig. 8b. The cross sections calculated for the pickup reaction to the $\frac{5}{2}_2^+$ level are included in fig. 10. The DWBA result (dashed curve) disagrees with the data both in shape and magnitude. Much better agreement with the data is obtained in the CCBA calculations. The shape of the cross section is well reproduced apart from some possible structure around 45°. The magnitude is also reasonable. The results obtained with parameter sets B and C differ mainly in magnitude, and changes in the magnitude are observed when the β_3 parameters in the entrance and exit channels are varied. Parameter set B and large values of β_3 are favored since the cross sections are underestimated. However, contributions from compound nucleus formation may well account for the difference(see below).

In order to obtain information about the relative importance of the various processes in the CCBA calculations, fig. 11 shows a decomposition of the transitions to

the $\frac{5}{2}_1^+$, $\frac{7}{2}^+$ and $\frac{5}{2}_2^+$ states into components. The individual contributions were obtained by allowing only single transitions to take place. Parameter sets A and B of table 2 were used ($\beta_3 = 0.085$ was used for the $\frac{5}{2}_2^+$ state). Certain transitions were found to play only a minor role and were therefore ignored (compare fig. 11 with fig. 10 where all transitions are included). The transitions which were disregarded are those to the $\frac{7}{2}^+$ state for the $\frac{5}{2}_1^+$ state cross section and those to the $\frac{5}{2}_1^+$ state for the $\frac{7}{2}^+$ state cross section.

The processes which involve two or more inelastic scatterings (the 3^- to $\frac{1}{2}^-$ routes shown as dash-dot curves) are generally weaker than those which proceed via a single inelastic scattering. Thus, the important contributions are the two (or more) step, processes with a single inelastic excitation before or after the transfer of a proton and, if possible, the direct one-step proton pickup process. All these processes contribute with similar magnitude. They also interfere coherently and affect strongly the results from the full CCBA calculation. Thus, strong modifications of the DWBA predictions are found, and deviations between experimental and theoretical spectroscopic

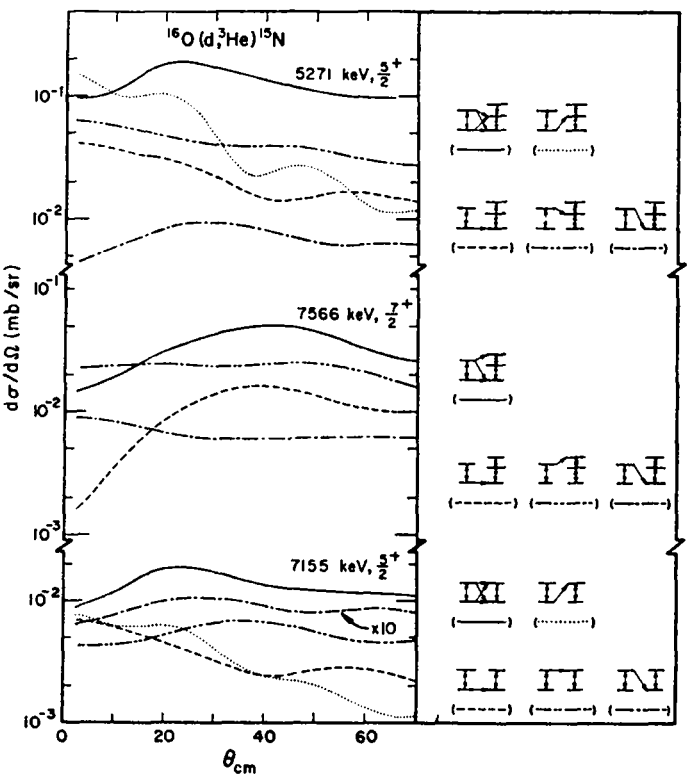

Fig. 11. Calculated CCBA angular distributions for the transitions to the 5271 keV $\frac{5}{2}_1^+$, 7566 keV $\frac{7}{2}^+$ and 7155 keV $\frac{5}{2}_2^+$ states. The solid curves are the result of the coherent superposition of the other curves which are obtained by allowing only the indicated transitions to take place.

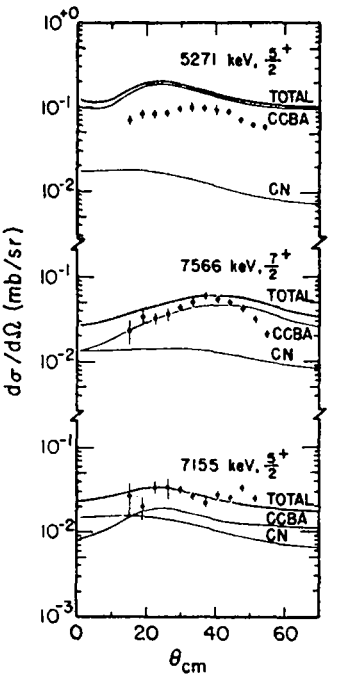

Fig. 12. Experimental and theoretical angular distributions for the transitions to the 5271 keV $\frac{5}{2}_1^+$, 7566 keV $\frac{7}{2}^+$ and 7155 keV $\frac{5}{2}_2^+$ states. The thin lines are the results of the CCBA and compound nucleus calculations as indicated and the thick lines represent their incoherent superposition.

factors in table 3 (e.g. for the $\frac{5}{2}_2^+$ or $\frac{7}{2}^+$ states) are not surprising.

Fig. 12, finally, shows the data for the three transitions together with the calculated distributions from the coupled-channel analysis and the compound nucleus analysis. The former are the results obtained with parameter set A, $\beta_3 = 0.6$ for the deuterons and parameter set B, $\beta_3 = 0.25$ or 0.085, respectively, for the ^{3}He particles (see fig. 10). The latter are the estimates obtained using constant-temperature level densities with $(\sigma/\sigma_{calc})^2 = 2$ (see fig. 5). The thick curves shown in fig. 12 represent the incoherent superposition of the two components.

The relative contributions from compound nucleus formation to the total cross sections are on the order of about 10, 25 and 45 %, respectively. The calculated CCBA curve for the 5271 keV $\frac{5}{2}_1^+$ state, which somewhat overestimates the measured cross sections, is practically unchanged. The CCBA curve for the 7566 keV $\frac{7}{2}^+$ state is increased slightly and results in an overestimate at the larger angles. For the 7155 keV $\frac{5}{2}_2^+$ state, the compound nucleus contributions are almost equal to the contributions from the coupled channels analysis and the incoherent superposition agrees very well with the experimental cross sections.

6. Summary

Angular distributions have been measured for the (d, ^{3}He) reaction on ^{16}O leading to states in ^{15}N up to an excitation energy of 10 MeV. Most cross sections are relatively weak except for the transitions to the $\frac{1}{2}^-$ ground state and the $\frac{3}{2}^-$ state at 6324 keV. These two states are thought to be mainly composed of a lp hole in the closed shell of ^{16}O.

It was felt that a compound nucleus reaction mechanism could play a role for the weak transitions. The calculations, however, suggested that only the cross section for the transition to the unresolved doublet near 9800 keV was mainly due to compound nucleus formation. The compound nucleus contributions to the other transitions are generally much smaller, and the average is about 30 % of the observed cross section. It should be noted, however, that predictions of absolute compound nucleus cross sections are difficult to make because of the uncertainties in the level densities and their spin dependence, which are required in the calculations.

Considering direct reaction mechanisms, it was found that only the two strong transitions agree well with the DWBA predictions. Poor fits were obtained for several of the other transitions with some spectroscopic factors much larger than theoretically predicted. The reason for this result became evident when the CCBA was employed, which allowed inelastic excitations of the 3^- octupole phonon in the entrance and/or the exit channel. Only the strong transition to the $\frac{1}{2}^-$ ground state showed similar results for DWBA and CCBA, although even here the magnitude differed slightly. Inelastic multi-step and direct processes are equally important for the weak transitions to the $\frac{5}{2}_1^+$ and $\frac{5}{2}_2^+$ states at 5271 and 7155 keV. The direct transfer strength for the transition to the $\frac{7}{2}^+$ state at 7566 keV was taken to be zero, and the calculated cross sections are therefore entirely due to inelastic multi-step processes. Including in addition the estimated compound nucleus cross sections, which was most important for the transition to the $\frac{5}{2}_2^+$ state, rather good agreement with the data was obtained for these three transitions. We may note that the transition to the $\frac{5}{2}_1^+$ state at 5271 keV was experimentally resolved from the nearby $\frac{1}{2}^+$ state thus allowing a detailed comparison with theoretical predictions.

It should be emphasized that the agreement between the CCBA calculations and the data was achieved using spectroscopic factors obtained from microscopic shell-model calculations without adjustment. Some microscopic spectroscopic factors differ by more than an order of magnitude from values obtained from the "DWBA fits". (Compare, for instance, cols. 11 and 15 of table 3.) In view of these results it was concluded that the use of the DWBA theory to estimate the amount of closed shell breaking by extracting spectroscopic factors for weak pickup transitions is highly questionable.

Thanks are due to W. E. Downer and the cyclotron staff for their assistance, and to K. T. Hecht for many discussions.

References

1) P. J. Ellis and L. Zamick, Ann. of Phys. **55** (1969) 61
2) A. P. Zuker, B. Buck and J. B. McGrory, Phys. Rev. Lett. **21** (1968) 39
3) S. S. M. Wong, Nucl. Phys. **A120** (1968) 625
4) P. J. Ellis and T. Engeland, Nucl. Phys. **A144** (1970) 161;
   T. Engeland and P. J. Ellis, Nucl. Phys. **A181** (1972) 368
5) A. Watt, B. J. Cole and R. R. Whitehead, Phys. Lett. **B**, to be published
6) J. C. Hiebert, E. Newman and R. H. Bassell, Phys. Rev. **154** (1967) 898
7) W. Bohne, H. Homeyer, H. Morgenstern and J. Scheer, Nucl. Phys. **A113** (1968) 97
8) H. Doubre, D. Royer, M. Arditi, L. Bimbot, N. Frascaria, J. P. Garron and M. Riou, Phys. Lett. **29B** (1969) 355
9) K. H. Purser, W. P. Alford, D. Cline, H. W. Fulbright, H. E. Gove and M. S. Krick, Nucl. Phys. **A132** (1969) 75
10) J. L. Snelgrove and E. Kashy, Phys. Rev. **187** (1969) 1246
11) D. Hartwig, Doctoral Thesis, Karlsruhe (1971), unpublished
12) D. Braunschweig, T. Tamura and T. Udagawa, Phys. Lett. **35B** (1971) 273
13) N. K. Glendenning and R. S. Mackintosh, Nucl. Phys. **A168** (1971) 575
14) R. S. Mackintosh, Nucl. Phys. **A170** (1971) 353
15) R. J. Ascuitto, N. K. Glendenning and B. Sørensen, Nucl. Phys. **A183** (1972) 60
16) R. J. Ascuitto and B. Sørensen, Nucl. Phys. **A190** (1972) 309
17) P. J. Ellis and A. Dudek, Particles and Nuclei **5** (1973) 1
18) S. Lie, T. Engeland and G. Dahll, Nucl. Phys. **A156** (1970) 449;
   S. Lie and T. Engeland, Nucl. Phys. **A169** (1971) 617
19) W. C. Parkinson, J. F. Petersen, R. H. Day, D. C. DuPlantis, W. S. Gray and J. Bardwick, Nucl. Instr. **119** (1974) 61
20) F. S. Goulding, D. A. Landis, J. Cerny and R. H. Pehl, Nucl. Instr. **31** (1964) 1
21) E. Silverstein, Nucl. Instr. **4** (1959) 53
22) J. T. Routti and S. G. Prussin, Nucl. Instr. **72** (1969) 125
23) M. A. Firestone, Ph.D. Thesis, The University of Michigan (1974), unpublished
24) L. Yaffe, Ann. Rev. Nucl. Sci. **12** (1962) 153
25) U. Hauser and W. Kerler, Rev. Sci. Instr. **29** (1958) 380
26) J. R. Comfort, Argonne National Laboratory Report PHY-1970B (1970), unpublished
27) W. Hauser and H. Feshbach, Phys. Rev. **87** (1952) 366
28) K. A. Eberhard, P. von Brentano, M. Böhning and R. O. Stephen, Nucl. Phys. **A125** (1969) 673;
   K. A. Eberhard and A. Richter, Proc. Int. Conf. on statistical properties of nuclei, Albany, NY 1971, ed. J. Garg (Pergamon Press, New York, 1971) p. 139
29) T. Ericson, Nucl. Phys. **11** (1959) 481
30) A. Gilbert and A. G. W. Cameron, Can. J. Phys. **43** (1965) 1446
31) P. J. Brancazio and A. G. W. Cameron, Can. J. Phys. **47** (1969) 1029
32) D. L. Hanson, R. G. Stockstad, K. A. Erb, C. Olmer and D. A. Bromley, Phys. Rev. **C9** (1974) 929
33) J. M. Blatt and V. F. Weisskopf, Theoretical nuclear physics (Wiley, New York, 1952)
34) D. Shapira, R. G. Stockstad and D. A. Bromley, Phys. Rev. **C10** (1974) 1063;
   L. Milazzo-Colli and M. G. Braga-Marcazzan, in Progress in nuclear physics, vol. 2, ed. D. M. Brink and J. H. Mulvey (Pergamon Press, New York, 1970) p. 145;
   U. Facchini and E. Saetta-Minichella, Energia Nucl. **15** (1968) 54
35) T. Ericson and T. Mayer-Kuckuk, Ann. Rev. Nucl. Sci. **16** (1966) 183
36) M. Maruyama, Nucl. Phys. **A131** (1969) 145
37) S. M. Grimes, J. D. Anderson, J. W. McClure, B. A. Pohl and C. Wong, Phys. Rev. **C6** (1972) 236
38) S. Ayik and J. N. Ginocchio, Nucl. Phys. **A234** (1974) 13
39) P. D. Kunz, University of Colorado, unpublished
40) D. J. Millener, to be published
41) R. J. Ascuitto and N. K. Glendenning, Phys. Rev. **181** (1969) 1396
42) D. J. Edens, D. Phil. thesis, Oxford (1970)

43) J. C. Hiebert, E. Newman and R. H. Bassel, Phys. Rev. **154** (1967) 898
44) T. Tamura, Rev. Mod. Phys. **37** (1965) 679
45) D. Nguyen, J. Phys. Soc. Jap. **21** (1966) 2462
46) F. Hinterberger, G. Mairle, U. Schmidt-Rohr, G. J. Wagner and P. Turek, Nucl. Phys. **A111** (1968) 265
47) G. Duhamel, H. Langevin-Joliot, J. P. Didelez, E. Gerlic and J. van de Wiele, Nucl. Phys. **A231** (1974) 349
48) B. G. Harvey, J. R. Meriwether, J. Mahoney, A. Bussiere de Nercy and D. J. Horen, Phys. Rev. **146** (1966) 712
49) A. M. Bernstein, in Advances in nuclear physics, vol. 3, ed. M. Baranger and E. Vogt (Plenum Press, New York, 1970) p. 325
50) G. C. Ball and J. Cerny, Phys. Rev. **177** (1969) 1466
51) A. Bussiere, N. K. Glendenning, B. G. Harvey, J. Mahoney, J. R. Meriwether and D. J. Horen, Phys. Lett. **16** (1965) 296
52) F. D. Becchetti, Jr. and G. W. Greenlees, in Proc. 3rd Int. Symp. on polarization phenomena in nuclear reactions, Madison, 1970, ed. H. H. Barschall and W. Haeberli (University of Wisconsin Press, Madison, 1971) p. 682